Intriguing climatic shifts in a 90 kyr old lake record from northern Russia

MONA HENRIKSEN, JAN MANGERUD, ALEXEI MATIOUCHKOV, ANDREW S. MURRAY, AAGE PAUS AND JOHN INGE SVENDSEN

BOREAS

Henriksen, M., Mangerud, J., Matiouchkov, A., Murray, A. S., Paus, A. & Svendsen, J. I. 2008 (February): Intriguing climatic shifts in a 90 kyr old lake record from northern Russia. *Boreas*, Vol. 37, pp. 20–37. 10.1111/j.1502-3885.2007.00007.x. ISSN 0300-9483.

A 22 m long sediment core from Lake Yamozero on the Timan Ridge in northern Russia has provided evidence of intriguing climatic shifts during the last glacial cycle. An overall shallowing of the lake is reflected in the lower part of the cores, where pollen indicates a transition from glacial steppe vegetation to interstadial shrub-tundra. These beds are capped by a well-defined layer of compact clay deposited in relatively deep water, where pollen shows surrounding spruce forests and warmer-than-present summer temperatures. The most conservative interpretation is that this unit represents the last interglacial period. However, a series of Optical Stimulated Luminescence (OSL) dates suggests that it corresponds with the Early Weichselian Odderade interstadial (MIS 5a). This would imply that the Odderade interstadial was just as warm as a normal interglacial in this continental part of northern Europe. If correct, then pollen analysis, as a correlation tool, is less straightforward and the definition of an interglacial is more complex than previously thought. We discuss the validity and possible systematic errors of the OSL dates on which this age model is based, but conclude they really indicate a MIS 5a age for the warm period. Above the clay is an unconformity, most likely reflecting a period of subaerial exposure implying dry conditions. Deposition of silt under fluctuating cold climates in the Middle Weichselian continued until a second gap in the record at *c*. 40 kyr BP. The lake basin started to fill up again around 18 kyr BP.

Mona Henriksen (e-mail: mona.henriksen@umb.no), Jan Mangerud and John Inge Svendsen, Department of Earth Science and Bjerknes Centre for Climate Research, University of Bergen, Allégaten 41, NO-5007 Bergen, Norway; present address for Mona Henriksen: Department of Plant and Environmental Sciences, Norwegian University of Life Sciences, P.O. Box 5003, No-1432 Ås, Norway; Alexei Matiouchkov, VSEGEI (National Geological Institute), Sredny proezd 74, St. Petersburg 199026, Russian Federation; Andrew S. Murray, Nordic Laboratory for Luminescence Dating, Department of Earth Sciences, University of Aarhus, Risø National Laboratory, DK-4000 Roskilde, Denmark; Aage Paus, Department of Biology and Bjerknes Centre for Climate Research, University of Bergen, Allégaten 41, NO-5007 Bergen, Norway; *received 12th September 2006, accepted 28th April 2007.*

The project Quaternary Environment of the Eurasian North (QUEEN) has timed the advances of the Barents–Kara and Scandinavian ice sheets onto the northern Russian mainland at *c*. 90–80 kyr, 60–50 kyr and 20 kyr BP (Svendsen *et al*. 2004). South of the ice sheets, cold and dry conditions prevailed, occasionally interrupted by milder periods between glacial advances (Hubberten *et al*. 2004; Velichko *et al*. 2004). The stratigraphic framework for the Pechora Lowland (Fig. 1) is based on a compilation of events found in a number of river bluffs and gravel pits each representing short time-windows in the geological record (e.g. Guslitser *et al*. 1985; Arslanov *et al*. 1987; Tveranger *et al*. 1995, 1998; Mangerud *et al*. 1999, 2001; Henriksen *et al*. 2001; Svendsen *et al*. 2004). The aim of this study was therefore to obtain a continuous palaeo-environmental record for this area covering the last interglacial–glacial cycle, i.e. 130 kyr. Previous studies have shown that most lakes in the Pechora Lowland were formed only 13–9 kyr ago by the melting of dead ice and permafrost (Henriksen *et al*. 2003; Paus *et al*. 2003). However, Lake Yamozero (Fig. 1) is located outside all Weichselian glacial limits (Svendsen *et al*. 2004) and can thus be expected to contain a longer sediment record. It was for this reason that this site was selected for the present study.

We use the stratigraphic nomenclature of Western Europe, where the Weichselian, Eemian and late Saalian periods correspond to marine isotope stages (MIS) 2–5d, 5e and 6, respectively. The Weichselian is subdivided into Early (MIS 5d–5a), Middle (MIS 4–3) and Late Weichselian (MIS 2). We correlate the Weichselian with the Russian Valdaian glacial period, the Eemian with the Mikulinian interglacial and the Saalian with the Moscovian glacial.

Lake Yamozero and surroundings

Lake Yamozero (65°01′N, 50°14′E) is situated at an altitude of 213 m a.s.l. on the eastern slope of the Timan Ridge, a low bedrock range with a maximum altitude of 471 m a.s.l. that forms the water divide between the Mezen and Pechora river basins (Fig. 1). The lake is located outside the present zone of permafrost (Brown *et al*. 1997). Mean July and January temperatures are 13°C and −17°C, respectively, and annual precipitation is 534 mm at the Levkinskaya weather station, *c*. 45 km to the southeast of Yamozero (http://meteo.infospace.ru/climate/html; National Snow and Ice Data Center 2006). The bedrock is made up of Precambrian metamorphic rocks and Devonian sandstones (Nalivkin 1973; Pachukovsky *et al*. 1978). Previous prospect coring revealed that the lake basin occupies a closed bedrock depression located above a heavily fractured

DOI 10.1111/j.1502-3885.2007.00007.x

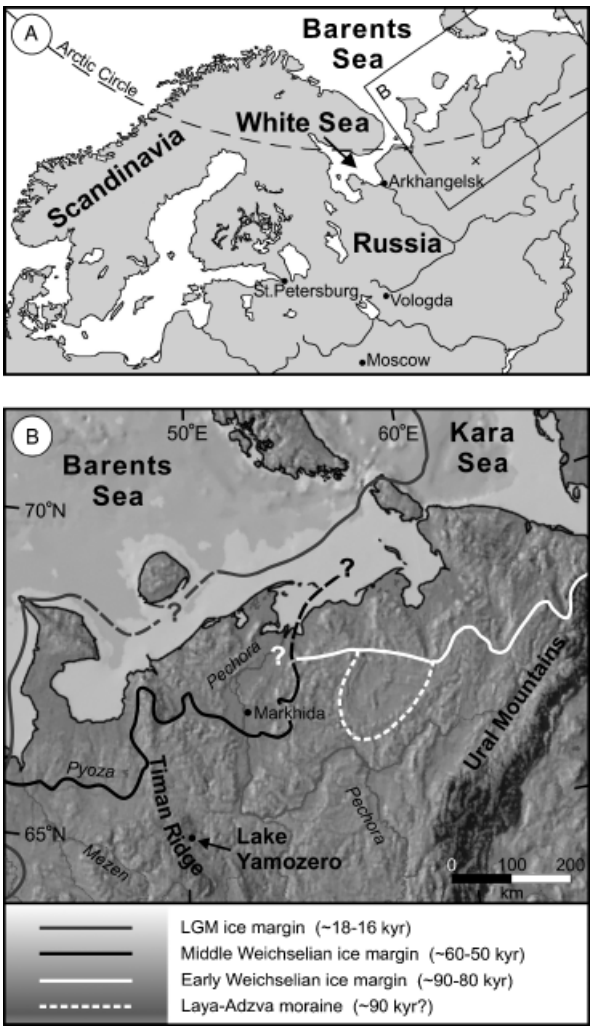

Fig. 1. A. Map of northern Europe. B. Map of northeastern European Russia. Lake Yamozero is located on the Timan Ridge between the Mezen and Pechora river basins. Also shown are Weichselian glacial limits for the Barents–Kara Ice Sheet according to Svendsen *et al.* (2004) and for the eastern limit of the Scandinavian Ice Sheet at LGM according to Demidov *et al.* (2006).

zone, and contains 50–60 m thick Quaternary sediments (Pachukovsky *et al.* 1978) (Figs 2, 3). The present lake covers an area of *c.* 30 km^2 and has an almost circular outline with a maximum water depth of *c.* 3 m. The small catchment area of 95 km^2 consists of mires near the shore and an open, boreal forest dominated by spruce higher up. A series of distinct shorelines encircles the lake up to a level of about 15 m above the present lake level (Fig. 2). The main inflow is from a creek entering the western side of the lake.

Methods

Lake coring

Coring was carried out from lake-ice in March 2000. A hand-driven, 'Russian' peat corer was used to sample the uppermost 2–3 m of sediments. For the deeper parts, we used heavy motorized geotechnical drilling equipment (UGB-50) belonging to the Usinsk Division of the Polar Ural Geological Expedition. Metre-long core segments with a diameter of 10 cm were recovered in PVC tubes mounted inside a steel coring tube. To obtain a complete record, two overlapping cores were collected from each site; nevertheless, some gaps occur in sandy sediments. Casing was used to prevent closure of the borehole; however, we were unable to press the casing more than 12 m into the sediments because the lake-ice was not strong enough. During sampling, some horizontal shear planes were created in the lake sediments when the core cutter rotated. Occasionally, the upper part of the metre-long cores was filled by sediments that were scraped in while the corer was being lowered. Usually, the dislocated 'trash' sediments were easily recognizable, as they were softer and lacked any horizontal stratification. This problem increased downwards into the sediment record, and we were unable to collect undisturbed samples below 22 m with the UGB-50 drilling equipment.

Sediment cores were obtained from three different sites on Lake Yamozero (Fig. 2). We obtained *c.* 14 m long cores from site 1 in the centre of the lake. At site 2 we only obtained a 3 m long core because the sediments consisted of sand. The best record was obtained from site 3, *c.* 2 km south of site 1, where a total thickness of 22 m was recovered. According to the previous prospect coring (Pachukovsky *et al.* 1978), the total sediment thickness above bedrock at this latter site is at least 40 m (Fig. 3).

Sediment analysis

The cores were transported unfrozen to Bergen for analysis. The core segments were first split lengthwise and described (Fig. 4). Undrained shear strength was determined applying a fall-cone test immediately after splitting of the cores. Water content and density of the sediments were measured in each core segment. Grain-size analyses were conducted using wet-sieving for the fraction coarser than 0.125 mm and a SediGraph 5100 for the more fine-grained fraction. A Munsell soil colour chart was used for sediment colour description. Weight loss on ignition (LOI) was used to estimate percentage organic and carbonate content (e.g. Heiri *et al.* 2001). Samples of 1–2 g of dry sediments were first dried overnight at 105°C and then incinerated at 550°C for 1 h, where loss of weight yielded organic content. Further loss when the samples were exposed to 950°C for 1 h yielded carbonate content. Composite logs for sites 1 and 3 (Fig. 5) were made.

Radiocarbon-dating

Handpicked plant remains with a dry weight of > 10 mg from site 3 were used for accelerator mass

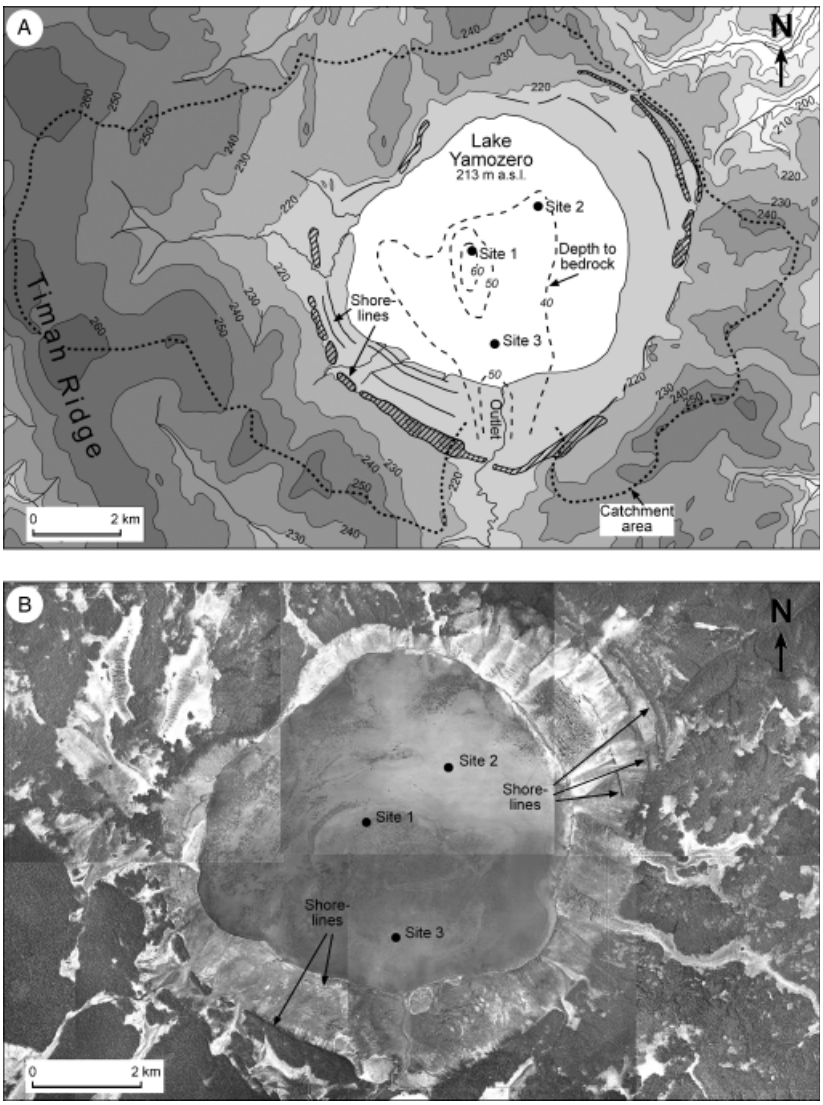

Fig. 2. A. Map of Lake Yamozero and surroundings. The catchment area (dotted line), shorelines of former high lake levels and coring sites are shown. Depths to bedrock are given in metres below lake level (from Pachukovsky *et al.* (1978)). Altitudes are given in m a.s.l., higher areas are darker. B. Mosaic of aerial photos of Lake Yamozero. The lake is surrounded by spruce forest and mires, and former shorelines encircle the lake.

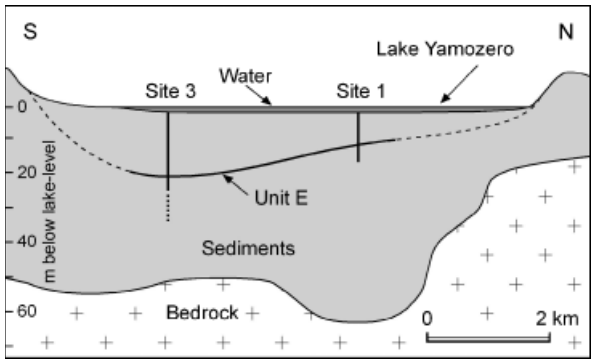

Fig. 3. A north–south profile of Lake Yamozero. Depth to bedrock is from Pachukovsky *et al.* (1978). The clay unit E is marked with tentative extensions. Also marked are the core depths at the two coring points (solid vertical lines). At site 3, an additional 12 m of sediments was penetrated by rods without sampling the sediments (dashed vertical line).

spectrometry (AMS) radiocarbon-dating. We tried to use only fresh-looking, terrestrial plant remains that could be identified. However, in some levels the content of terrestrial plant remains was very low, and for certain samples we had to include aquatic macrofossils in order to get enough organic material for AMS ^{14}C dating (Table 1).

Luminescence dating

One of the cores from site 3 was split and sampled in a photographic darkroom for Optically Stimulated Luminescence (OSL) dating. Twenty samples of 5–15 cm thick sediment slices were cut from different levels in the core segments and subsequently dated at the Nordic Laboratory for Luminescence Dating (Table 2). Equivalent doses were measured using the Single

Fig. 4. Photo of core segments between 18.6 and 19.4 m at site 3; cf. Fig. 5.

Aliquot Regenerative (SAR) dose protocol (Murray & Wintle 2000) applied to 90–180 μm quartz grains. The dose rates were determined using laboratory gamma spectrometry (Murray *et al.* 1987; Olley *et al.* 1996). The exposed half of the core segments was soaked in water for a day to obtain saturated water content (percentage of dry weight). The effects of saturated water content and calculated cosmic ray contributions are included in the dose rate data.

Pollen

A pollen diagram was constructed from the 22 m long record at site 3. The pollen samples (1 cm^3), with *Lycopodium* tablets added for estimates of concentration (Stockmarr 1971), were prepared by standard methods (Fægri & Iversen 1989). The diagram, including 161 samples, was drawn using the computer program CORE 2.0 (Kaland & Natvik 1993). The percentage calculation basis (ΣP) comprises the terrestrial pollen taxa. For a taxon X within Cyperaceae, aquatics, spores and reworked microfossils, the calculation basis is ΣP+X. The diagram was subdivided into local pollen assemblage zones (paz) by visual inspection and labelled Y-1 to Y-18.

Results

Lithostratigraphy and dates

The sediment stratigraphy is shown in Fig. 5 in composite logs from sites 1 and 3. Lithostratigraphical units are labelled A to H from the base.

Unit A: Silty sand. – Unit A consists of horizontally stratified silty sand with some gravel, the sediments probably accumulating in shallow water near the lake margin. Alternatively, it may represent sediment gravity flows. Three OSL dates from this unit yielded 54–59 kyr, while a fourth gave 79 kyr (Table 2).

Unit B: Clay. – This is a well-defined layer of fine-grained sediment with sharp lower and upper contacts. It consists of laminated silt and clay at site 1 and of massive clay containing a few scattered pebbles and some plant remains at site 3. The finer grained sediments suggest deposition in deeper water.

Unit C: Silty sand. – The lower part of unit C is dominated by laminated sandy silt and sand coarsening upwards to gravelly, silty sand. Towards the top, it becomes finer again (Fig. 5). The unit is more fine-grained at site 3 than at site 1. The gravel could have been brought into the deeper part of the basin by gravity flows or it could have accumulated in shallow water near the lake margin. Unit C is dated by OSL to 96 and 111 kyr (Table 2).

Unit D: Organic silt and gyttja. – This unit, 80 cm thick at site 3, is characterized by the highest organic content below the Holocene. The lowermost part consists of brownish, laminated silt with some scattered pebbles interbedded with laminae of organic matter. The organic content increases upwards as the sediment grades into a dark, laminated silty gyttja capped by a coarse detritus gyttja (Fig. 4). We assume that the sediments accumulated in a lake that gradually became shallower and more productive. The inorganic laminae may reflect flooding episodes. At site 1, unit D is only 6–10 cm thick and consists of thin layers of gyttja interbedded with silt (Fig. 5); the shallower position indicates exposure of this site. An infinite ^{14}C age (Table 1) and OSL ages of 49, 71 and 72 kyr were obtained from unit D (Table 2).

Unit E: Clay. – Unit E is a well-defined, 15–25 cm thick layer consisting of a firm, nearly massive silty clay. The upper contact is erosional. Although unit E is found *c.* 10 m shallower at site 1 than at site 3 (Fig. 5), the similar lithology indicates deposition from suspension in relatively deep water at both sites. OSL dating of this unit was not possible owing to the lack of sand-sized quartz grains.

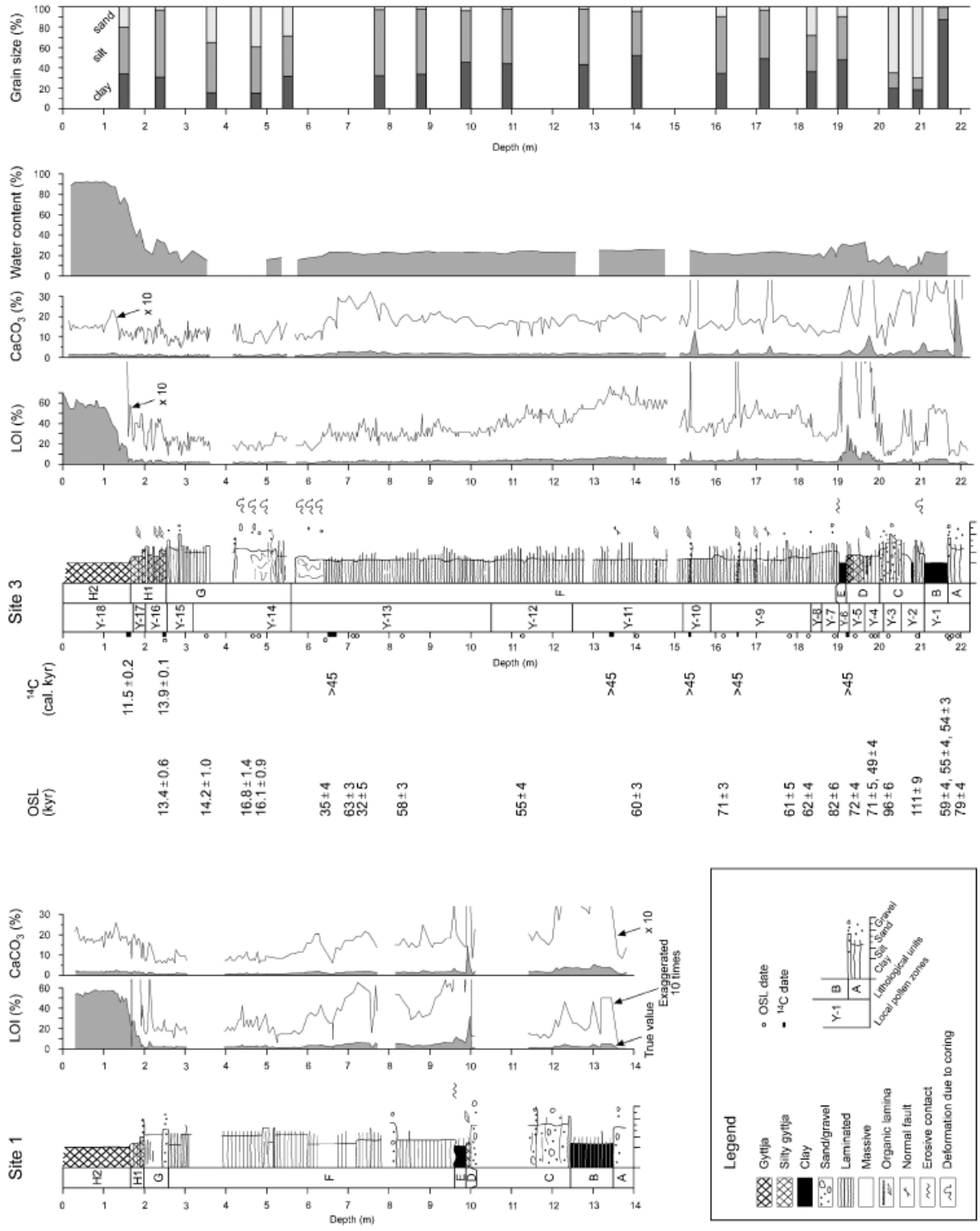

Fig. 5. Composite logs from site 1 and site 3 (Fig. 2). The logs are plotted on the same depth scale measured from the lake floor at *c.* 1.5 m water depth at both sites. Distance between the sites is *c.* 2 km. The lithostratigraphic units are indicated by letters (A–H), and pollen zones at site 3 by numbers (Y-1 to Y-18). As the logs are composite, there are some small discrepancies of the plotted depths of the radiocarbon and OSL dates compared to the depth listed in Tables 1 and 2.

Table 1. Radiocarbon dates. The laboratories are: ETH - Zürich, Switzerland; Beta Analytic Inc., USA. The dates are calibrated with CALIB version 5.0.2 using the IntCal04 calibration data set (Reimer *et al.* 2004).

Lab. no.	Sample no. PECHORA	Depth (cm)	Unit	Material dated	^{14}C age $\pm 1\sigma$ (years BP)	δ^{13}C (‰)	Max and min (*mean*) of cal. age ranges, 1σ (years BP)
ETH-25567	28-02/50	156–166	H2	Leaves, fruits, twigs and catkin, mainly of *Betula nana* (some burnt)	9985 ± 75	-26.1	11 610–11 290 (*11 450 ± 160*)
ETH-26290	28-03/40	244–252	H1	Fragments of *Betula* leaves and some fruits and catkin, leaves, twigs and pieces of bark	$11\,995 \pm 90$	-30.7	13 950–13 770 (*13 860 ± 90*)
ETH-26291	29-05/95	650–670	F	Weathered twigs, bark and stems, some might be aquatic	$> 45\,000 \pm 400$	-30.2	$> 45\,000$
ETH-25569	29-12/45	1340–1350	F	Stems of *Luzula* and *Poaceae*; bark, twigs of *Saxifraga*?, insects, and fruits of *Salix*, *Papaver* and Brassicaceae	$40\,510 \pm 845$	-25.8	$> 45\,000$
ETH-25570	29-14/30	1534–1539	F	Mosses, bark, fruits of *Carex*, weathered twig.	$> 45\,000 \pm 360$	-27.7	$> 45\,000$
ETH-23901	29-15/38	1654–1655	F	Mainly aquatic *Drepanocladus*	$43\,700 \pm 1120$	-26.9	$> 45\,000$
Beta-142505	29-17	1905–1912	D	Leaves and *Scirpus lacustris* fruits	$48\,130 \pm 1300$	-28.7	$> 45\,000$

Unit F: Laminated silt. – Unit F is an up to 13 m thick sequence of dark grey, laminated silt. The unit is sandier at site 1, although the lowermost 50 cm at site 3 is also sandy with scattered pebbles. Between 18 m and 15 m at site 3 there are some distinct sand laminae as well as scattered plant remains. The organic content is low, but LOI values are up to 11% between 18 m and 13 m (Fig. 5). Unit F is interpreted as lacustrine sediments deposited mainly from suspension with occasionally mass-flow events depositing the sandier horizons. Four ^{14}C dates yielded infinite ages (Table 1), while 10 OSL ages range from 32 to 82 kyr partly in reverse order and partly with a large spread, especially in the upper part of the unit (Table 2).

Unit G: Sandy silt. – This is a sandy silt unit with some gravel, partly massive and partly laminated. The entire sequence probably accumulated on the floor of a shallow lake, where the massive sediments may have been influenced by wave action and grounded lake-ice. Correlation between the sites and individual cores was not straightforward. The core gap at site 3 is possibly slightly wider than shown in Fig. 5. Two OSL dates in the lower part of unit G yielded 16.1 and 16.8 kyr, and a sample *c.* 1 m further up 14.2 kyr (Table 2).

Unit H: Organic silt and gyttja. – This uppermost unit, 2–3 m thick, is divided into H1 and H2. Unit H1 consists of laminated organic silt interbedded with sandy layers, whereas H2 consists of massive gyttja. The organic sediments accumulated at the floor of a relatively shallow, eutrophic lake, whereas the minerogenic laminae in unit H1 probably result from flooding episodes. From overlapping levels in the lower part of H1, a ^{14}C date yielded $13\,860 \pm 90$ cal. yr and an OSL date $13\,400 \pm 600$ yr (Tables 1, 2). A ^{14}C date from the lower part of unit H2 yielded $11\,450 \pm 160$ cal. yr BP, i.e. at onset of the Holocene.

Pollen stratigraphy

A pollen diagram of selected taxa is given in Fig. 6; some taxa from pollen assemblage zone (paz) Y-3 to Y-6 are shown in an enlarged diagram (Fig. 7). In Table 3, each paz is named by dominant taxa and/or taxa showing percentage maxima within the paz.

Paz Y-1 contains high proportions of reworked microfossils, e.g. pre-Quaternary pollen and spore types, which together with poor pollen preservation prevents a reliable interpretation. In paz Y-2, reworked microfossils decrease dramatically, whereas *Salix*, *Artemisia*, *Carex* and total concentration (8×10^4 grains/cm^3) increase. Paz Y-3 represents a return to extremely low pollen concentration and many reworked microfossils.

Paz Y-4 shows increasing aquatics and pollen concentration (5×10^4 grains/cm^3). In paz Y-5, trees, aquatics and total pollen concentration decrease in the first half, whereas *Betula* (60% ΣP) and total pollen concentration values increase at the end of paz Y-5.

Paz Y-6 is different from all other pre-Holocene zones, with maxima in *Populus*, *Juniperus* and *Salix* in the first half, and especially the maxima of *Picea* (50% ΣP) and broad-leaf trees in the last half, indicating summer temperatures warmer than present. Total pollen concentration reaches 8×10^5 grains/cm^3.

The abrupt transition to paz Y-7 supports the existence of the hiatus postulated on top of clay unit E. Pollen preservation deteriorates, reworked microfossils increase and total pollen concentration decreases. In paz Y-8, reworked microfossils show maximum percentages and total concentration is at a minimum (2×10^2 grains/cm^3).

Table 2. Optically simulated luminescence (OSL) dates on quartz using the sand grain fraction (w.c. = water content). All dates are from the Nordic Laboratory for Luminescence Dating, Aarhus University, Risø, Denmark.

Risø lab. no.	Field no. PECHORA	Depth (cm)	Unit	Sediments, comments	Age ± 1σ (kyr)	Equivalent dose (Gy)	*n*	Annual dose rate (Gy/kyr)	w.c. (%)
022529	27-01/75-80	250–255	H1	Silty gyttja interbedded with sand	13.4 ± 0.6	23.7 ± 0.5	18	1.77 ± 0.07	44
022530	27-02/85-90	349–354	G	Laminated sandy silt	14.2 ± 1.0	27.2 ± 1.3	24	1.91 ± 0.09	18
022531	27-03/80-85	462–467	G	Massive to faintly laminated sandy silt	16.8 ± 1.4	31 ± 2	23	1.83 ± 0.08	17
022532	27-03/95-100	477–482	G	Massive to faintly laminated sandy silt	16.1 ± 0.9	31.4 ± 0.8	24	1.95 ± 0.09	16
022533	27-05/10-15	640–645	F	Laminated silt and clay	35 ± 4	75 ± 8	23	2.14 ± 0.08	31
032501	27-05/85-95	715–725	F	Laminated silt and clay	63 ± 3	145 ± 4	21	2.31 ± 0.09	29
022534	27-05/95-100	725–730	F	Laminated silt and clay. Poor date due to little quartz	32 ± 5	77 ± 12	18	2.37 ± 0.12	27
012561	27-06/90-95	830–835	F	Laminated silt and clay	58 ± 3	123 ± 6	27	2.11 ± 0.06	34
012562	27-09/80-85	1123–1128	F	Laminated silt and clay	55 ± 4	131 ± 6	15	2.40 ± 0.12	29
012563	27-12/56-63	1403–1410	F	Laminated silt and clay with relatively high LOI	60 ± 3	130 ± 5	24	2.18 ± 0.07	37
012564	27-14/22-27	1589–1594	F	Laminated silt and clay	71 ± 3	144 ± 1	24	2.13 ± 0.08	28
022535	27-15/77-82	1755–1760	F	Laminated silt and clay	61 ± 5	132 ± 8	24	2.21 ± 0.09	33
022536	27-16/15-20	1800–1805	F	Laminated silt and clay	62 ± 4	109 ± 4	21	1.76 ± 0.08	24
012565	27-16/80-85	1865–1870	F	Laminated silt and clay	82 ± 6	190 ± 11	33	2.39 ± 0.09	24
012566	27-16/97-104	1882–1889	E	Compact silty clay. Not enough quartz for dating				2.51 ± 0.10	41
012567	27-17/34-39	1913–1918	D	Silty gyttja	72 ± 4	108 ± 4	26	1.66 ± 0.08	55
032503	27-17/75-80	1954-1959	D	Silty layer within gyttja silt	71 ± 5	125 ± 6	27	1.76 ± 0.09	29
032502	27-17/80-90	1959–1969	D	Silty layer within gyttja silt	49 ± 4	117 ± 4	21	2.34 ± 0.15	29
022537	27-18/4-9	1995–2000	C	Silty sand with some organic matter	96 ± 6	120 ± 5	24	1.25 ± 0.06	21
012568	27-18/64-69	2055–2060	C	Silty sand	111 ± 9	121 ± 5	39	1.09 ± 0.08	19
032506	27-19/70-75	2135–2140	A	Silty sand	59 ± 4	132 ± 6	21	2.24 ± 0.10	23
032505	27-19/75-80	2140–2145	A	Silty sand	55 ± 4	129 ± 6	21	2.33 ± 0.12	23
032507	27-19/80-85	2145–2150	A	Silty sand	54 ± 3	128 ± 5	21	2.38 ± 0.11	23
012569	27-19/95-100	2160–2165	A	Silty sand	79 ± 4	166 ± 5	21	2.09 ± 0.09	14
OSL dates from Markhida									
022590	02-4093	1900		Shallow marine sand below till	41 ± 3	25.8 ± 1.1	21	0.63 ± 0.04	27
052566	02-4094	1800		Shallow marine sand below till	71 ± 5	54 ± 2	26	0.76 ± 0.04	24
022591	02-4102	1350		Shallow marine sand below till	68 ± 5	58 ± 3.3	18	0.85 ± 0.04	28
022592	02-4103	1250		Shallow marine sand below till	65 ± 6	53 ± 4	21	0.81 ± 0.04	27
022593	02-4107	640		Shallow marine sand below till	66 ± 4	90 ± 3	20	1.36 ± 0.06	28
022594	02-4108	650		Shallow marine sand below till	59 ± 3	87 ± 2	21	1.49 ± 0.06	27
022595	02-4109	660		Shallow marine sand below till	53 ± 3	68 ± 1.7	21	1.27 ± 0.05	27
022596	02-4110	670		Shallow marine sand below till	58 ± 4	75 ± 4	19	1.30 ± 0.07	34
022597	02-4113	780		Shallow marine sand below till	61 ± 4	56 ± 2	27	0.92 ± 0.04	27
022598	02-4114	830		Shallow marine sand below till	70 ± 6	58 ± 4	24	0.83 ± 0.04	26
022599	02-4115	980		Shallow marine sand below till	68 ± 6	39 ± 2	27	0.57 ± 0.04	26

Paz Y-9 shows increasing total concentration ($5–12 \times 10^4$ grains/cm^3) and reduced values of *Sphagnum*, fern spores and reworked microfossils. In paz Y-10, *Betula* (12% ΣP) decreases before regaining dominance in Y-11 (50% ΣP), where the percentages of Ericales and total pollen concentration ($2–3 \times 10^5$ grains/cm^3) reach distinct maxima.

At the transition to Y-12, *Betula* (35% ΣP) total concentration decreases, while *Picea*, *Artemisia* and *Botryococcus* rise. In Y-13, *Betula* (25% ΣP) total

concentration continues to decrease, whereas *Alnus* and reworked microfossils increase. Total concentration ($1–2 \times 10^4$ grains/cm^3) continues to fall in Y-14, and *Carex*-type and *Pediastrum* increase.

Abrupt changes at the Y-14/Y-15 transition point to an erosional unconformity. Y-15 shows pollen assemblage similarities with Y-4, including maxima in *Salix*, *Juniperus* and the aquatics *Potamogeton* and *Pediastrum*. However, total pollen concentration in Y-15 (2×10^4 grains/cm^3) is lower. Slightly increasing total concentration in Y-16 involves maxima in birch and juniper, whereas *Artemisia* and *Dryas* show minimum values.

Y-17 reflects decreasing birch, juniper and total concentration (2×10^4 grains/cm^3) and increasing *Dryas* and *Sinapis*-type. The uppermost paz, Y-18, shows rapid changes by the dominance of birch, spruce and *Pediastrum*. Early local maxima of juniper, *Salix* and *Urtica* are replaced by *Populus*, *Pinus*, *Alnus* and *Filipendula* in the last half.

Geochronology

The OSL ages (Table 2) from units G and H are consistent with the Lateglacial age inferred from the

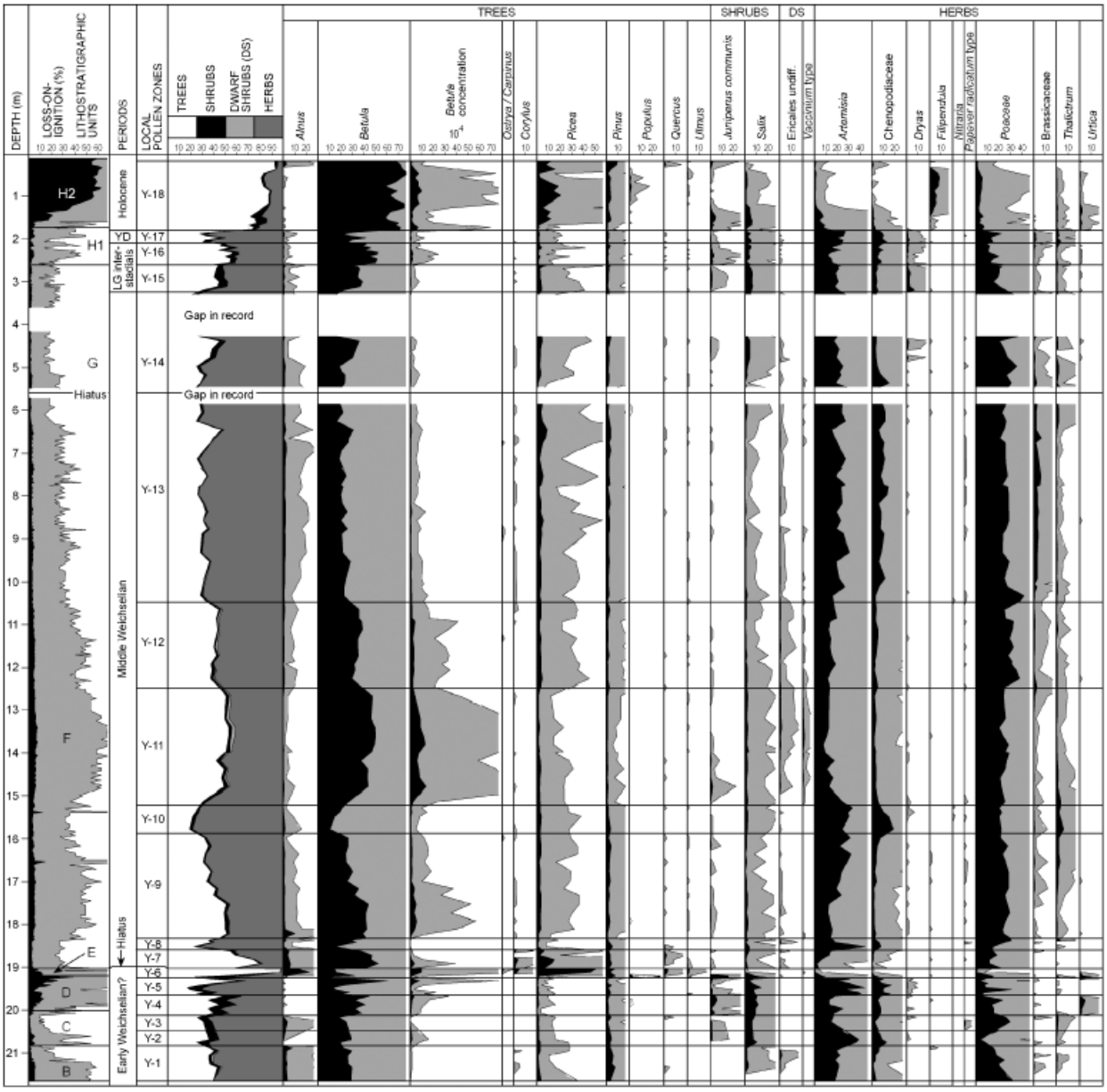

Fig. 6. Pollen percentage diagram of selected taxa from site 3, Lake Yamozero, plotted versus sediments depth. The lithostratigraphic units are given to the left together with LOI. Taxa characteristics of each paz are given in Table 3. The light grey shade pattern represents 10 × exaggeration of the scale. In addition, pollen concentrations (grains cm^{-3}) of total pollen and *Betula* are shown.

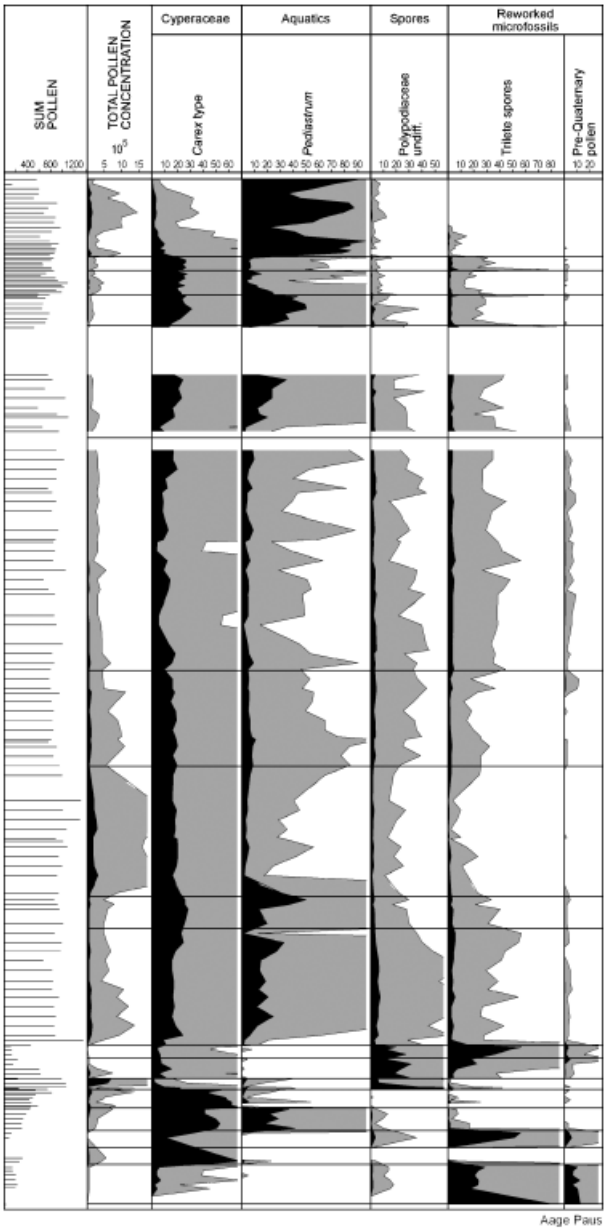

Fig. 6. Continued.

calibrated ^{14}C dates (Table 1); in fact, at 2.5 m depth a ^{14}C date and OSL date overlap within 1 SD. In the strata below, all ^{14}C dates are infinite, while OSL dates display a large scatter (Fig. 8), making the chronostratigraphic framework for this part more uncertain. Nevertheless, the OSL dates suggest that unit F is of Middle Weichselian age. However, for units A–E we present two conflicting age models (Fig. 8): 1) the 'warmer-than-present' unit E is of Eemian age and 2) unit E is younger than the Eemian.

Age model 1

It is commonly assumed that summer temperatures in northern Europe were never as warm as at present between the Eemian and the Holocene (e.g. Velichko *et al.* 1984; Helmens *et al.* 2000; Guiter *et al.* 2003). If this postulate is correct, then unit E (paz Y-6) represents the Eemian, because the pollen stratigraphy of this unit indicates warmer-than-present summers. This conclusion is supported by similar flora development in Y-6, as described for the Early Eemian in other parts of European Russia (e.g. Devyatova 1982; Grichuk 1984; Velichko *et al.* 2004), and a high lake level, as also described for the Early Eemian on the Central Russian Plain (Alyoshinskaya & Gunova 1976; Gey *et al.* 2001). The pollen stratigraphy indicates that Y-6 was deposited during the first 2–3 kyr of the Eemian, i.e. before 125 kyr ago. This suggests a hiatus of about 50 kyr, represented by an erosional unconformity, between units E and F, if unit F started to accumulate about 70 kyr ago (Fig. 8).

An implication of this age model is that units A–D are of Late Saalian age. The cooling indicated by paz Y-5 may then correlate with the Zeifen–Kattegat climate oscillation (e.g. Seidenkrantz *et al.* 1996; Caspers *et al.* 2002; Kukla *et al.* 2002). A similar cooling is also recorded on the Central Russian Plain (e.g. Semenenko *et al.* 1981; Zelikson 1995). Another implication is that all OSL ages below unit E must be rejected as too young (Figs 8, 9C).

Age model 2

In this age model, we accept the OSL ages as largely correct, although it is clear that for some dates the uncertainties are underestimated. Nine OSL ages from sediments below the warmer-than-present unit E yield a mean value of 72 kyr, which is more than 60 000 years younger than predicted by age model 1. In age model 2, we therefore conclude that unit E represents an unexpected warm interstadial that is younger than the Eemian, probably the Early Weichselian interstadial Odderade (85–74 kyr, MIS 5a). This model relies entirely on the reliability of the OSL dates and we therefore discuss these dates thoroughly.

How reliable are the OSL dates?

If age model 1 is correct, then at least all nine OSL ages from the underlying strata are wrong, whereas if this series of OSL ages as a whole gives a meaningful result, then age model 2 is supported. We have previously obtained several hundred OSL ages from exposed sections in this part of Russia and the current chronostratigraphic framework for the glacial history relies heavily on this method (Mangerud *et al.* 1999, 2001, 2004; Henriksen *et al.* 2001; Pavlov *et al.* 2001; Astakhov 2004; Svendsen *et al.* 2004). Our experience is that when many OSL ages are obtained from contemporary sediment sequences the results show a near normal distribution with a mean age broadly consistent with expectations, but unexplained outliers occur (Mangerud

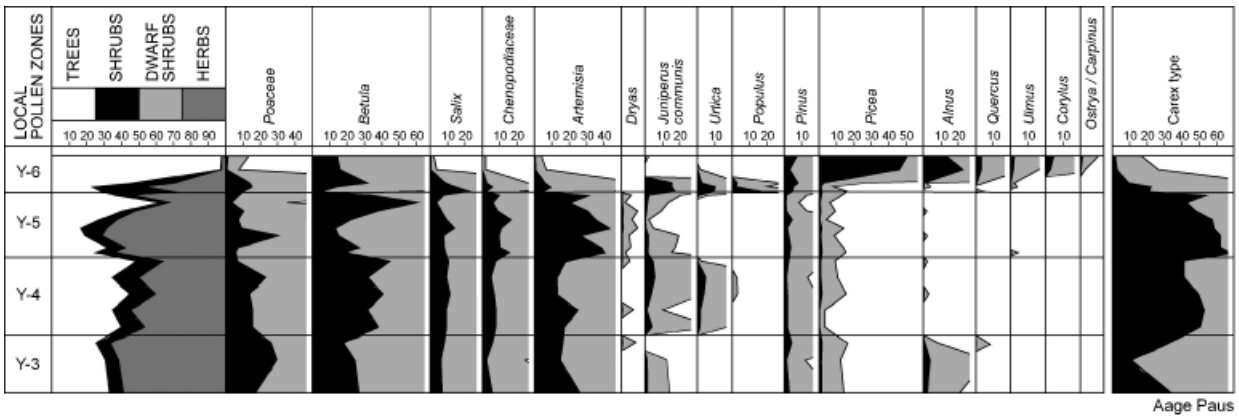

Fig. 7. Enlarged segment of pollen zones Y-3 to Y-6 (pollen percentage diagram). The light grey shade pattern represents 10 × exaggeration of the scale.

Table 3. Local pollen assemblage zones (paz) of Lake Yamozero and their dominant taxa and/or taxa showing percentage maxima in the paz.

PAZ	Taxa characteristics
Y-18	*Betula-Picea-Filipendula-Pediastrum*
Y-17	*Artemisia*-Chenopodiaceae-Poaceae
Y-16	*Betula-Juniperus*-Chenopodiaceae
Y-15	*Betula-Salix-Dryas-Pediastrum*
Y-14	*Salix-Artemisia*-Poaceae
Y-13	*Artemisia*-Chenopodiaceae-*Sinapis*
Y-12	*Betula-Picea*-Poaceae-*Pediastrum*
Y-11	*Betula*-Ericales
Y-10	Chenopodiaceae-*Thalictrum-Carex*
Y-9	*Betula-Artemisia-Carex-Pediastrum*
Y-8	*Artemisia*-Chenopodiaceae-*Sphagnum*-pre-Quaternary pollen
Y-7	*Betula-Picea-Sphagnum*-Polypodiaceae
Y-6	*Alnus-Picea-Urtica*
Y-5	*Artemisia-Dryas-Carex*
Y-4	*Betula-Juniperus-Urtica-Pediastrum*
Y-3	*Papaver*-Poaceae-pre-Quaternary pollen
Y-2	*Salix-Artemisia-Carex*
Y-1	*Pinus-Artemisia*-pre-Quaternary pollen

et al. 2004; Murray *et al*. 2007). In Fig. 9D–F we plotted three other series of OSL ages from the Pechora Basin. The dates from Eemian shallow marine sand (Murray *et al*. 2007) and also from the ice-dammed Lake Komi (Mangerud *et al*. 2004) are clearly older than the dates below unit E (Fig. 9C). The dates from the shallow marine sand below the Markhida moraine overlap with the dates from both below and above unit E. In view of the good correspondence of the OSL ages with the radiocarbon chronology in the upper part of the sequence (Fig. 8) and with radiocarbon and other independent age control from elsewhere in the region (Mangerud *et al*. 1999; Pavlov *et al*. 2001), it would be surprising if all the ages below unit G were much too young. Nevertheless, it is a fact that the scatter in this data set is larger than predicted from the calculated uncertainties. We discuss potential sources of error associated with the OSL dating method below.

Incomplete bleaching. – If sediments are not completely reset by exposure to daylight before deposition, then the OSL dates will overestimate the age of the most recent burial. This is often presented as a potential source of error in the dating of material from glacial or periglacial environments, but it is very unlikely to be a major problem in this age range (Murray & Olley 2002), and in any case would result in an overestimate of age rather than an underestimate.

Estimation of annual dose rate. – A marked characteristic of this core is the large variation in dose rate in units A–E (below *c*. 19 m) compared with units F–H (Table 2, Fig. 10A). Uncertainties in the true average dose rates certainly explain some of the scatter in the data set. For instance, the dose rate for sample 032502 is 2.34 ± 0.15 Gy/kyr, whereas immediately above and below this sample the dose rate is significantly lower, i.e. 1.76 ± 0.09 and 1.25 ± 0.06 Gy/kyr (Table 2). It is unlikely that the beta particle contribution to the dose rate is in error, because the range of a beta particle is less than a few millimetres; the beta dose rate is *c*. 2/3 of the total dose rate. However, only *c*. 50% of the gamma dose rate is derived from within 15 cm of the layer of interest; the remaining 50% comes from sediment at a greater distance. It is not known how steep the gamma dose rate gradient around sample 032502 is, and so numerical corrections cannot be made for this effect. Nevertheless, it is likely that the true average dose rate to this layer is smaller than given for this layer alone. If a gamma dose rate based on the immediately overlying and underlying layers is used instead of that derived from analysis of the layer itself, the age of 032502 changes from 49 ± 4 kyr to 55 ± 3 kyr; the true age presumably lies somewhere between these two values. Similarly, the apparent age of sample 012568 will change

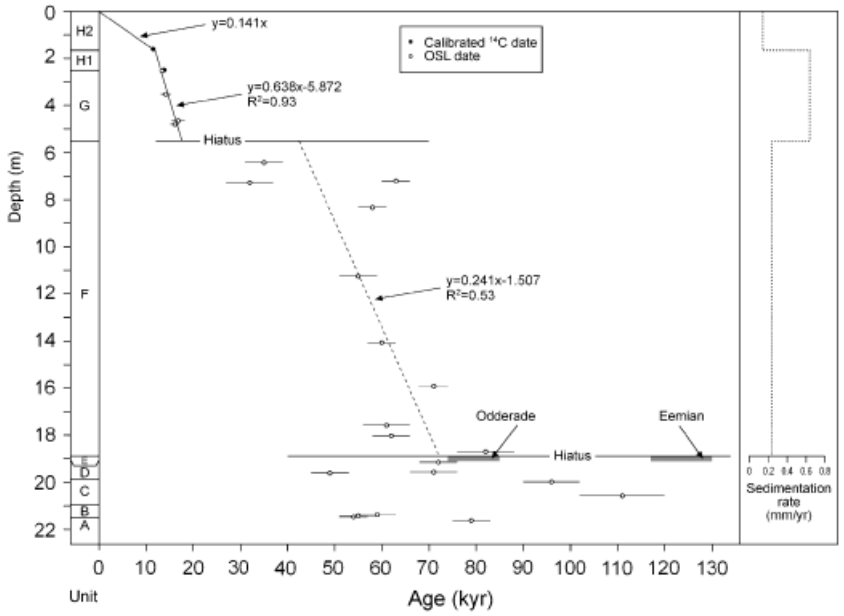

Fig. 8. Age-depth curve for site 3. Dates are shown with 1 SD. The ages of the Odderade interstadial and Eemian interglacial are shown at the stratigraphic level of the 'warm-climate' unit E. The right panel shows average sedimentation rates for units F–H based on the linear regression lines in the left panel.

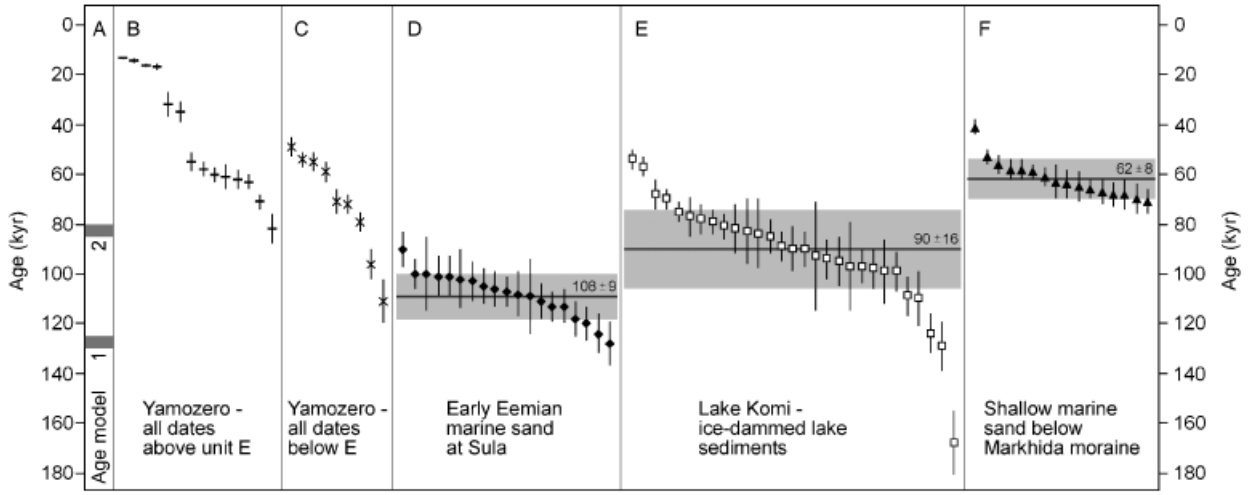

Fig. 9. A. Stratigraphic position of the two age models discussed in the text. B. OSL dates from units above the warmer-than-present unit E (Table 2, Fig. 8). C. OSL dates from units below unit E (Table 2, Fig. 8). D. OSL dates from Early Eemian shallow marine sediments in the Pechora Lowland (Murray *et al.* 2007). E. OSL dates from ice-dammed Lake Komi sediments in the Pechora Lowland (Mangerud *et al.* 2004). F. OSL dates from shallow marine sediments beneath the Markhida moraine in the Pechora Lowland (Table 2), described as 'alluvial sand A' in Mangerud *et al.* (1999). Means (horizontal line) and standard deviations (shaded) are also given in panels D–F.

from 111 ± 9 to 88 ± 6 kyr. However, it is important to realize that these are the two most extreme cases in this data set, and that in any case the true error will be much less than these limiting values. In addition, the overall effect of such errors in estimation of the gamma contribution to the total dose rate is to increase the variability in the ages, but probably not produce a systematic error, i.e. the average age for a unit containing several OSL ages would remain relatively unchanged if the dose rates were better estimated, only the spread between individual dates would be reduced.

Water content and compaction. – The age estimates assume that the water content has remained unchanged from deposition to the present. Although the sediments in Lake Yamozero have probably always been water saturated, compaction would have decreased the water content with time. Higher water content would reduce the time-averaged dose rates, and thus increase the OSL age. As a general rule, a reduction of the water content by about 1% will increase the calculated OSL age by 1%. It seems unlikely that compaction occurred uniformly throughout the site's lifetime. In units A–E, in particular, almost all compaction probably took place when the water level dropped sufficiently to allow the erosion surface between units E and F to develop. In either age model, this was early in the burial period, so the water contents measured today would be representative

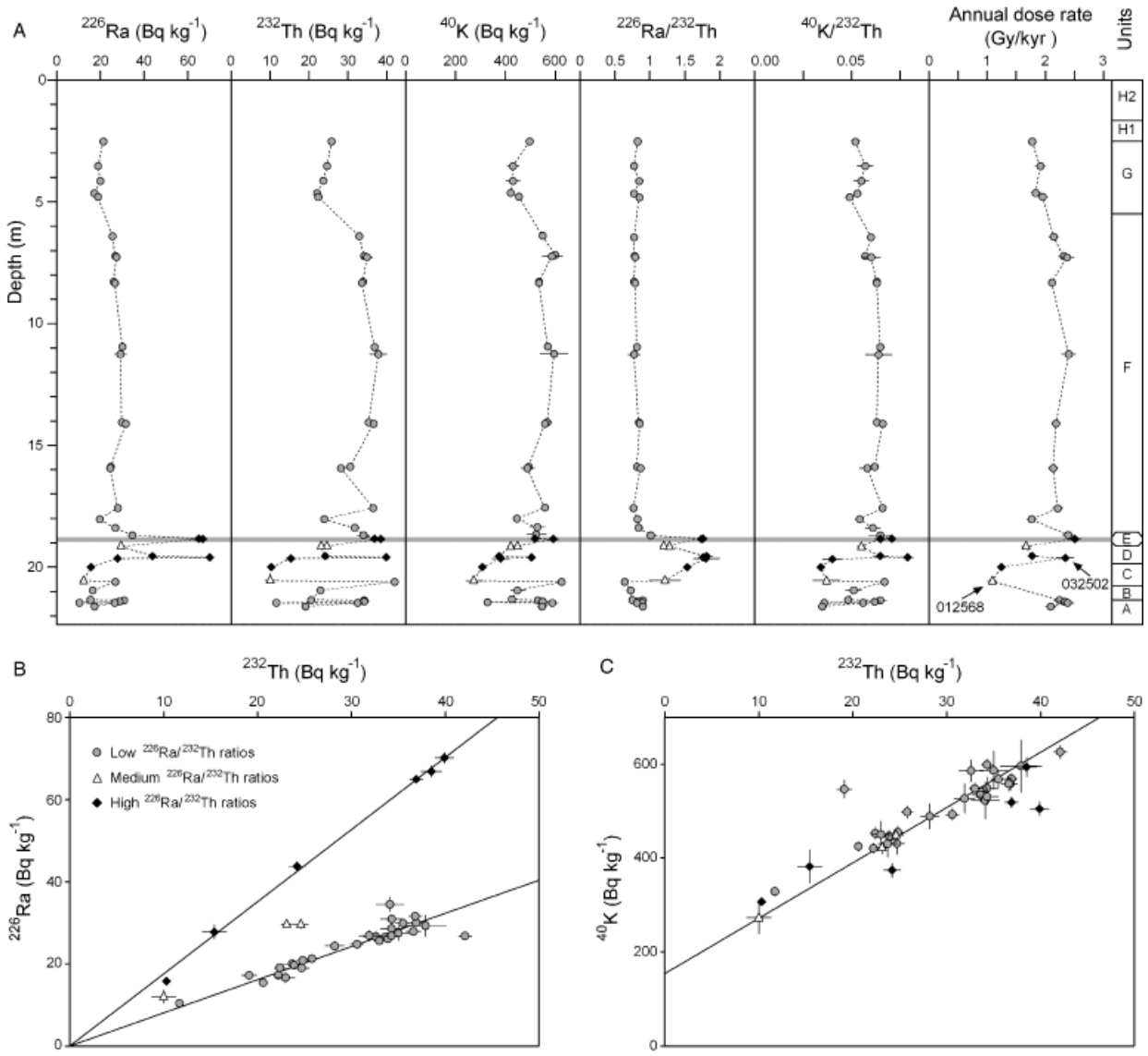

Fig. 10. A. Down-core variation of radioactivity used for calculation of the dose rates. Grey horizontal line marks unit E. Circles, triangles and diamonds represent low, intermediate and high $^{226}Ra/^{232}Th$ ratios, respectively. B. Values of ^{226}Ra plotted against ^{232}Th. C. Values of ^{40}K plotted against ^{232}Th.

of the values throughout the majority of the burial period. The ages of the deepest units could hardly be wrong by more than a few percent due to this effect.

Movement of radioactive isotopes. – Radionuclides may have moved between layers. If they moved from upper to lower layers during drying of the lake this would tend to lead to an underestimate of the dose rate in the upper layers (overestimating the real age) and too high a dose rate in the lower layers (underestimating the real age). In alternative 2, this could explain some of the overlap of dates above and below unit E. Most of the variation in radionuclide concentrations with depth is in and immediately below unit E (*c.* 19 m). This is true especially if the ratios of radium and potassium to thorium are considered. It is clear from Fig. 10 that there is a single radium to thorium ratio associated with layers between 18.8 and 19.95 m depth (unit E), and a lower distinct ratio both above and below these layers. There are three intermediate values, two at 19.2 m depth and one at 20.6 m, presumably reflecting post-depositional mixing or variation in sediment source. Radium is known to be immobile in fresh water (Hancock & Murray 1996), and given its short half-life of 1600 years it is therefore very likely to be in secular equilibrium with its parent ^{230}Th. Thus, the plot of radium against thorium can be interpreted as a plot of ^{230}Th (uranium series) against ^{232}Th (thorium series), and the change in ratio around unit E is taken to reflect a change in sediment source (Olley & Murray

1994). Given the constancy of the ratio above and below unit E, it is unlikely that this ratio has changed in any time-dependent manner. Since ^{232}Th is highly particle reactive (Moore 1992), and so most unlikely to be mobilized, one can reasonably assume that both thorium isotopes have remained immobile through time, and thus that the radionuclide mobility is unlikely to have been significant.

SAR approach. – Partly as a result of the dating problems that arose when analysing this core material, we tested our methodology (especially the SAR approach) by dating a marine formation in this part of Russia that is confidently ascribed to an early stage of the Eemian, i.e. around 130–125 kyr ago (Murray *et al.* 2007). In this case, the results obtained with the SAR method underestimate the real ages by no more than 14% (Fig. 9D), which is consistent with results obtained earlier from Eemian marine sands in Denmark (Murray & Funder 2003). On the other hand, Watanuki *et al.* (2005) present evidence that quartz can be accurate to at least beyond 300 kyr. It is therefore not yet clear where such a systematic error derives, or whether it applies to all sites in this age range; there is no evidence to suggest that any systematic uncertainty is variable from sample to sample, as would be required to produce the scatter observed in the ages from unit E and below.

In summary, it is possible to argue for the presence of some systematic error in our OSL ages, but in our view this is most unlikely to be $> 20\%$. We therefore conclude that the mean age for the units below E of *c.* 72 kyr is very unlikely to be more than 86 kyr, firmly excluding a pre-Eemian age.

Favoured age model and implications

The most conservative interpretation would be to accept age model 1, i.e. that unit E with the warmer-than-present forest vegetation (paz Y-6) is correlative with the Early Eemian. We do not consider that we have falsified this hypothesis, but, as concluded above, the OSL ages indicate a much younger age. The entire 'pre-radiocarbon range' glacial history of northern Russia is based on OSL dates. We therefore decided to explore the implications of age model 2, namely that the base of the core is about 90 kyr old and unit E is correlative with the Odderade interstadial. For the rest of the article we therefore postulate that unit E is of Odderade age.

This challenges current reconstructions of climatic development during the last glacial cycle for northern Europe. However, our knowledge of the climate history of the interior and northern part of the continent is at best fragmentary. Here, summer temperature responds more directly to insolation; summer insolation at this latitude (65°N) was not much lower during MIS 5a and 5c than during 5e (Berger & Loutre 1991). If an Odderade age of unit E is correct, this suggests a steeper and more pronounced east–west climate gradient for Europe.

For unit F and units G and H we simply used linear regressions that take into account all dates (Fig. 8), although the scatter of ages in unit F shows that some of them are probably wrong. Nevertheless, all dates suggest that sedimentation of unit F occurred between 72 and 42 kyr ago after about a 10 kyr long hiatus between units E and F, while unit G started to accumulate around 18 kyr ago, indicating another hiatus of about 20 kyr between units F and G (Fig. 8). The Younger Dryas–Holocene transition at around 11.5 kyr BP corresponds with the boundary between H2 and H1.

Palaeoenvironments

Dramatic changes during the Early Weichselian

Age model 2 indicates that units A–D accumulated during the cold Rederstall stadial (93–85 kyr, MIS 5b) and unit E during the early Odderade interstadial (Fig. 11). While the sandy units A and C were probably deposited in shallow water, the massive structure and fine-grained composition of unit B may suggest a lower sedimentation rate at deeper water depth (cf. Coakley & Rust 1968; Lemmen *et al.* 1988). The gyttja in unit D most likely accumulated in a shallow, productive lake (Fig. 11), where site 1 was probably for a time exposed subaerially. The overlying compact clay of unit E is the only pre-Holocene sediment with no difference in grain size between the two coring sites (Fig. 5), indicating accumulation in deep water. We speculate that unit E may be contemporaneous with the highest shoreline at 15 m above present lake level (Fig. 2), suggesting a total water depth of *c.* 35 m.

During deposition of the lower part of the record, the surrounding vegetation consisted of steppe with *Artemisia*, Chenopodiaceae and *Poaceae*, although patches of moister soils, as indicated by *Salix* and *Carex*-type pollen, are reflected in Y-2 (Fig. 6). A high content of reworked microfossils in Y-1 and Y-3 shows heavy soil erosion within the catchment, suggesting unstable soils and no trees growing locally. The reconstructed vegetation in unit D implies a change to a slightly warmer climate (paz Y-4) with tundra vegetation, including the shrubs *Juniperus* and *Salix* (Fig. 7). The presence of *Urtica* indicates fertile soils locally. A deteriorating climate is shown in Y-5 reflecting tundra/steppe vegetation with *Artemisia*, Chenopodiaceae, *Salix* and *Dryas*. It is noteworthy that the organic content in this part of the sequence increases upwards despite the cooling trend, probably reflecting decreasing size of the lake.

Starting in the uppermost part of unit D and continuing into unit E, the Y-5 birch maximum is followed by Y-6 shrub (*Juniperus*, *Populus* and *Salix*) maxima and subsequently a new birch maximum (Fig. 7). As

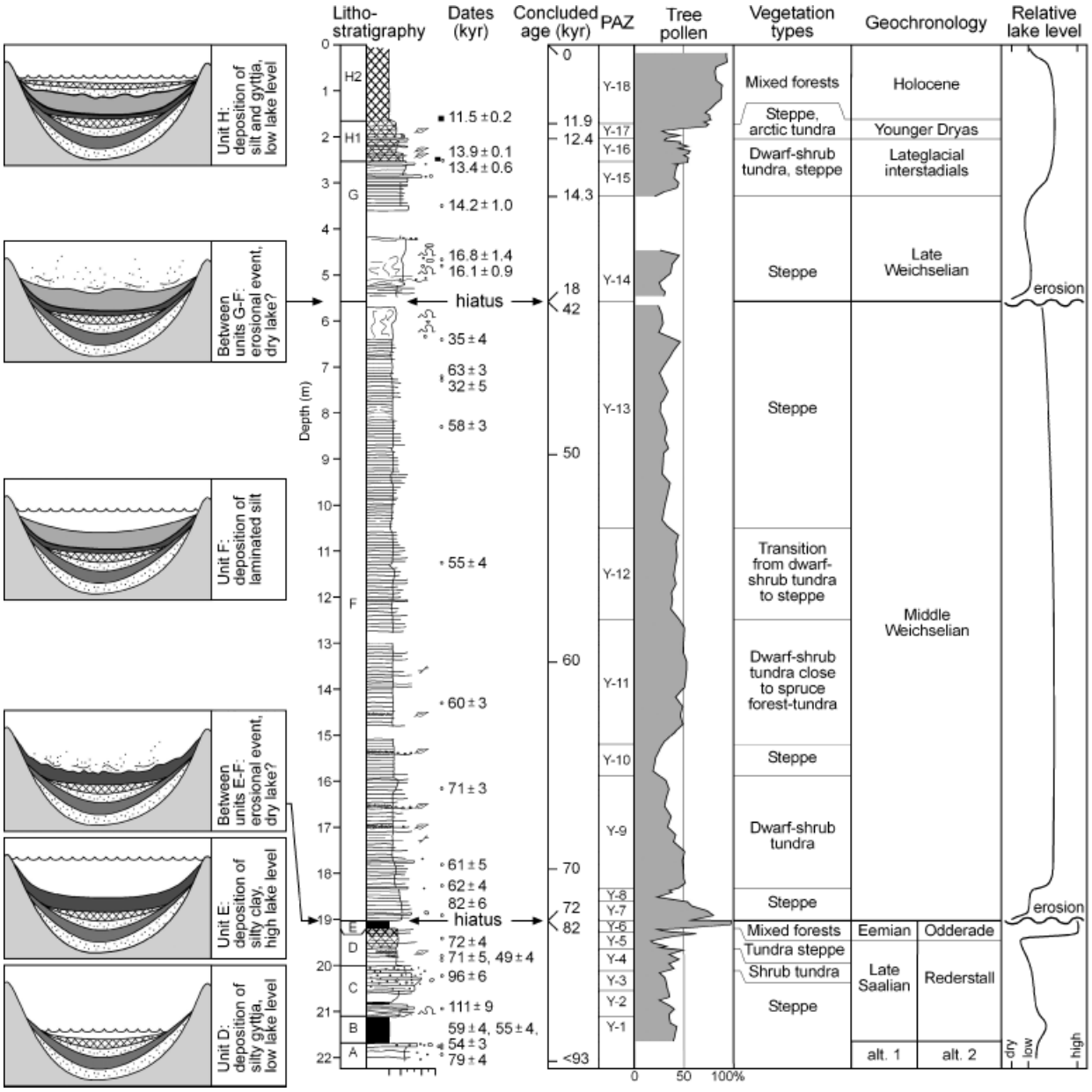

Fig. 11. Development of Lake Yamozero. From left to right: schematic development of Lake Yamozero shown in six time slots from units D to H; lithostratigraphic log with dates (for legend see Fig. 5); concluded age model (alternative 2); tree pollen (including *Betula nana*) and vegetation types; geochronology including the two alternative age models; relative lake level.

this pattern could reflect vegetation succession, the oldest birch maximum is interpreted as reflecting dwarf birch, whereas the latter should represent local tree birches. Local forest establishment is also indicated by high pollen concentrations. Lastly, forests dominated by *Picea* became established. The pollen assemblage suggests that stands of deciduous trees such as *Corylus*, *Alnus*, *Quercus* and *Ulmus* may have been present on drier and more fertile soils. A few pollen grains of *Carpinus* were found in the uppermost part of the zone, and some *Tilia* pollen was identified in core site 1 by inspection (correlation purposes). These deciduous trees are regional signals of warmer summers than at present. Increased precipitation associated with warmer and moister climate may have caused the rise in lake level. Perhaps amplified precipitation and/or the rising lake level caused an erosion episode connected with the peak in Mesozoic trilete spores in the lowermost part of Y-6 (Fig. 6).

Unit E probably correlates with an interstadial with up to 30–40% spruce pollen along the Pyoza River, some 140 km to the NE of Lake Yamozero (Fig. 1), dated to 89–75 kyr (Houmark-Nielsen *et al.* 2001). Along the upper reaches of the Yenisei River,

chernozem soils developed in loess during the Early Weichselian interstadials, although thinner than the interglacial chernozem (Haesaerts *et al.* 2005). Similar warm, interglacial conditions have been dated to *c.* 85 kyr ago in Arctic Canada (Miller *et al.* 1999).

The sharp upper contact of unit E is interpreted as an erosional surface which coincides with the abrupt changes from Y-6 to Y-7 (Fig. 6). Although situated *c.* 2 km apart and at approximately 10 m different depth in the sediment column (Figs 2, 5), unit E is eroded down to the same stratigraphic level at both coring sites, most likely caused by subaerial exposure and wind erosion (Fig. 11). Desiccation is also the simplest explanation why this unit is more compacted than the sediments below and above.

The environment during the Middle Weichselian

After formation of the erosive surface, the lake basin again filled up with water (unit F in Fig. 11). The low pollen concentration and high values of reworked microfossils in Y-7 and Y-8 (Fig. 6) point to colder conditions causing unstable soils and widespread steppe/deserts.

Paz Y-9 to Y-13 are interpreted as representing ameliorating climate and the establishment of a mostly treeless and grass-dominated vegetation mosaic, including dwarf-shrub tundra with *Betula nana* and *Dryas*, steppe/desert with *Artemisia* and Chenopodiaceae, and arctic tundra with *Papaver* and *Polemonium*. However, the high pollen concentrations and birch values (45–50% ΣP) in Y-9 (early part) and Y-11 could reflect milder periods and the establishment of local forest tundra/open birch forests (cf. Paus 1995). In Y-11, the disappearance of *Papaver* indicates stabilized soils, whereas the shrubs and dwarf shrubs became especially well developed (Fig. 6), probably forming the field and shrub layers of the local tree-birch vegetation. Y-11 also includes sparse finds of *Picea* stomata, indicating the development of spruce-forest tundra in the vicinity (Clayden *et al.* 1997). These warmer periods may correlate with the deglaciated phase around 65–60 kyr BP (Mezen transgression), where marine molluscs suggest that shallow water temperatures in the White Sea were only slightly cooler than today (Jensen *et al.* 2006) (Fig. 12). Paz Y-10 and Y-13 show progressive development of local steppe/desert vegetation with increased *Artemisia* and Chenopodiaceae at the expense of the dwarf shrubs. Finds of *Nitraria* accord the development of dry soils.

Late Weichselian development

The lower, more massive part of unit G started to accumulate around the time of the Last Glacial Maximum, and severe, periglacial conditions are indicated by paz

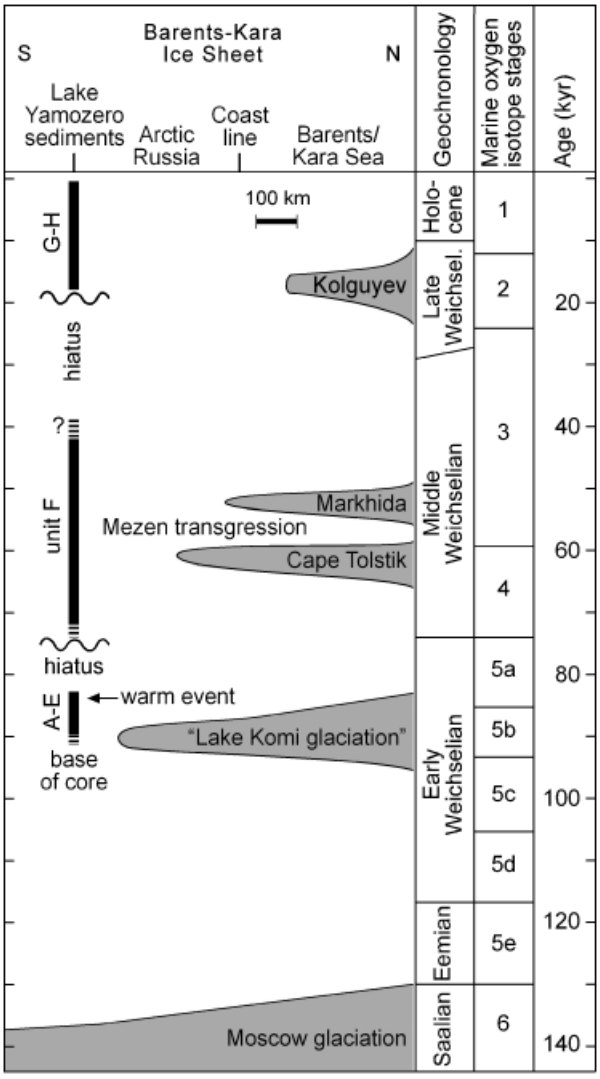

Fig. 12. Glaciation curve for the southern flank of the Barents–Kara Ice Sheet drawn as a profile through the southern Barents Sea and Pechora Lowland. Periods with preserved sediments and erosional events in Lake Yamozero are indicated.

Y-14 containing distinct amounts of reworked microfossils. Unit G has a relatively high content of sand (Fig. 5) and the highest sedimentation rate (Fig. 8), probably partly produced by winnowing in shallow water (Fig. 11) and partly by wind blown sand; high aeolian activity is recorded elsewhere in northern European Russia at this time (e.g. Velichko *et al.* 1984; Mangerud *et al.* 1999, 2002; Gey *et al.* 2001; Astakhov & Svendsen 2002).

Paz Y-15 and Y-16, dated to the Lateglacial Interstadial (Bølling–Allerød), reflect mosaic vegetation with patches of dwarf-shrub vegetation, with *Betula nana*, *Salix* and *Dryas*, and tundra/steppe vegetation, with *Artemisia*, *Hedysarum* and *Polemonium*. In Y-16, moister conditions may be indicated by the better developed dwarf-shrub tundra; increased birch values (45–50% ΣP) and total pollen concentration could also reflect the

development of sparse tree-birch vegetation. The pollen content of Y-17 (Younger Dryas) is characterized by steppe/desert and arctic-tundra elements (*Artemisia*, Chenopodiaceae, *Sinapis*-type, *Papaver*, *Hedysarum*) indicating cold and arid conditions. Snowbed vegetation is indicated by *Koenigia* and *Oxyria* (Fig. 6). Similar development has been recorded in many places in northern European Russia (e.g. Grichuk 1984; Velichko *et al*. 1997; Arslanov *et al*. 1999; Davydova *et al*. 2001; Gey *et al*. 2001; Hubberten *et al*. 2004), including further north on the Timan Ridge (Paus *et al*. 2003).

The Holocene warming

During the Holocene, Yamozoro was a shallow lake where gyttja accumulated. In paz Y-18 the development of open birch forests is indicated by high values of birch percentages and pollen concentration. These forests included shrubs such as *Juniperus* and *Salix*, with *Urtica* as a fertile-soil indicator. Thereafter, *Picea* established and mixed forests with *Betula*, *Picea*, *Populus* and, lastly, *Alnus* and *Pinus* developed (Fig. 6). *Filipendula* replaced *Urtica* as a fertile-soil indicator. This development ends with the present local taiga spruce forest. The sparse vegetated rim around the lake (Fig. 2) suggests a recent lowering of the lake level of approximately 5 m.

Correlation with the ice-sheet history

The age of the oldest Weichselian expansion of the Barents–Kara Ice Sheet onto the Pechora lowland is mainly based on OSL dates (Fig. 9E) of sediments from the ice-dammed Lake Komi, which formed in front of the ice sheet (Mangerud *et al*. 2001, 2004). Model experiments suggest a cold climate around Lake Komi, with summer temperatures about 5 °C colder than at present (Krinner *et al*. 2004). According to our age model 2, this glaciation predates unit E (Figs 9, 12).

It has been suggested that a sizeable ice cap was centred on the Timan Ridge 75–70 kyr ago, and that the hiatus between units E and F was caused by this ice cap covering Lake Yamozero (Larsen *et al*. 2006). However, the lack of till, glaciotectonic disturbance, but mainly that the erosion reached the same stratigraphic level of unit E at both coring sites, means that we reject this hypothesis.

Two re-advances of the Barents–Kara Ice Sheet occurred during the early Middle Weichselian, separated by an ice-free period with the Mezen marine transgression (Kjær *et al*. 2003; Svendsen *et al*. 2004; Larsen *et al*. 2006) (Figs 9F, 12). These glaciations probably correlate with periods of cold and dry conditions when steppe vegetation dominated in unit F at Lake Yamozero (Fig. 11).

The last major glaciation occurred during the Late Weichselian when the southern margin of the Barents–Kara Ice Sheet was located some 450 km to the north of Lake Yamozero (Polyak *et al*. 2000; Gataullin *et al*. 2001; Svendsen *et al*. 2004), and the Scandinavian Ice Sheet some 300 km to the west (Larsen *et al*. 1999; Demidov *et al*. 2006). We correlate the massive part of unit G with steppe vegetation surrounding Lake Yamozero with this glaciation (Fig. 12). Modelling suggests that the climate in this area was extremely cold and dry (Siegert & Marsiat 2001).

Conclusions

The 22 m long core record of lacustrine sediments from Lake Yamozero reveals lake levels varying from 15 m above to 19 m below present level; on two occasions, low lake levels have caused major hiati in the record. Reconstruction of the climate shows two transitions from cold, glacial conditions to warm, forested periods in the lower and uppermost parts of the core; in the middle part, generally cold conditions prevailed, with surrounding steppe or shrub-bush tundra vegetation. During the lower, warm, event the lake was surrounded by spruce forest, with deciduous trees on drier and more fertile soils indicating warmer summers than present. In a conservative age model, this warm event is correlated to the Eemian interglacial (MIS 5e). If correct, then a large number of OSL dates, which suggest a much younger age, have to be discarded. However, by critically evaluating all known sources of errors we found they could allow maximum 20% increase in the obtained OSL ages. We therefore conclude that the OSL dates suggest that this warm event correlates with the Odderade interstadial (MIS 5a) rather than with the Eemian. This indicates that, in the interior continental parts of northern Europe, summers of interstadials may be just as warm as interglacials, challenging current reconstructions of climatic development during the last glacial cycle. However, more investigations are needed to confirm whether or not this is correct.

Acknowledgements. – Andrei Monayev and the Usinsk Division of the Polar Ural Geological Expedition organized transport and the coring operations; Jozef Kusior and Stig Monsen helped in handling the cores in Bergen; Valery Astakhov helped with organizing the field expedition and with helpful comments; Hilary H. Birks identified macrofossils for AMS dating; Jan Berge prepared the pollen samples and Beate Ingvartsen drew the pollen diagram. Barbara Wohlfarth, Andrei A. Andreev and Jan A. Piotrowski constructively reviewed our work. To all these persons and institutions we extend our sincere thanks. This article is a contribution to the Russian–Norwegian interdisciplinary projects Paleo Environment and Climate History of the Russian Arctic (PECHORA II) and Ice Age Development and Human Settlement in northern Eurasia (ICEHUS) funded by the Research Council of Norway.

References

Alyoshinskaya, Z. V. & Gunova, V. S. 1976: Lake Nero history as a reflection of dynamics of the surrounding landscape. *In* Kalinin, G.

P. & Klige, L. (eds.): *Problemy paleogidrologii*, 214–222. Nauka, Moscow (in Russian).

Arslanov, K., Lavrov, A. S., Potapenko, L. M., Tertychanaya, T. V. & Chernov, S. B. 1987: New data on geochronology and paleogeography of the Late Pleistocene and Early Holocene in the northern Pechora lowland. *In* Punning, J. M. (ed.): *Novye dannye po geokhronologii chetvertichnogo perioda*, 101–111. Nauka, Moscow (in Russian).

Arslanov, Kh., Saveljeva, L. A., Gey, N. A., Klimanov, V. A., Chernov, S. B., Chernova, G. M., Kuzmin, G. F., Tertychnaya, T. V., Subetto, D. A. & Denisenkov, V. P. 1999: Chronology of vegetation and paleoclimatic stages of northwestern Russia during the late glacial and Holocene. *Radiocarbon 41*, 25–45.

Astakhov, V. 2004: Middle Pleistocene glaciations of the Russian North. *Quaternary Science Reviews 23*, 1285–1311.

Astakhov, V. I. & Svendsen, J. I. 2002: Age of remnants of a Pleistocene glacier in Bolshezemelskaya Tundra. *Doklady Akademii Nauk 384*, 1–5 (in Russian).

Berger, A. & Loutre, M. F. 1991: Insolation values for the climate of the last 10 million years. *Quaternary Science Reviews 10*, 297–317.

Brown, J., Ferrians Jr., O. J., Heginbottom, J. A. & Melnikov, E. S. 1997: *Circum-Arctic Map of Permafrost and Ground-Ice Conditions*. 1:10,000,00 Map CP-45. U.S. Geological Survey.

Caspers, G., Merkt, J., Müller, H. & Freund, H. 2002: The Eemian interglaciation in northwestern Germany. *Quaternary Research 58*, 49–52.

Clayden, S. L., Cwynar, L. C., MacDonald, G. M. & Velichko, A. A. 1997: Holocene pollen and stomates from forest-tundra on the Taimyr Peninsula, Siberia. *Arctic and Alpine Research 29*, 327–333.

Coakley, J. P. & Rust, B. R. 1968: Sedimentation in an arctic lake. *Journal of Sedimentary Petrology 38*, 1290–1300.

Davydova, N. N., Subetto, D. A., Khomutova, V. I. & Sapelko, T. V. 2001: Late Pleistocene–Holocene paleolimnology of three northwestern Russian lakes. *Journal of Paleolimnology 26*, 37–51.

Demidov, I. N., Houmark-Nielsen, M., Kjær, K. H. & Larsen, E. 2006: The last Scandinavian Ice Sheet in northern Russia: Ice flow pattern, decay dynamics. *Boreas 35*, 425–443.

Devyatova, E. I. 1982: *Late Pleistocene Natural Environments and Its Impact on Human Population in the Severnaya Dvina Basin and in Karelia*. 156 pp. Institute of Geology, Petrozavodsk (in Russian).

Fægri, K. & Iversen, J. 1989: *Textbook of Pollen Analysis*. 328 pp. John Wiley, Chichester.

Gataullin, V., Mangerud, J. & Svendsen, J. I. 2001: The extent of the Late Weichselian ice sheet in the southeastern Barents Sea. *Global and Planetary Change 31*, 453–474.

Gey, V., Saarnisto, M., Lunkka, J. P. & Demidov, I. 2001: Mikulino and Valdai palaeoenvironments in the Vologda area, NW Russia. *Global and Planetary Change 31*, 347–366.

Grichuk, V. P. 1984: Late Pleistocene vegetation history. *In* Velichko, A. A. (ed.): *Late Quaternary Environments of the Soviet Union*, 155–178. University of Minnesota Press, Minneapolis.

Guiter, F., Andrieu-Ponel, V., de Beaulieu, J. L., Cheddadi, R., Calvez, M., Ponel, P., Reille, M., Keller, T. & Goeury, C. 2003: The last climatic cycles in Western Europe: a comparison between long continuous lacustrine sequences from France and other terrestrial records. *Quaternary International 111*, 59–74.

Guslitser, B. I., Duragina, D. A. & Kochev, V. A. 1985: The age of the topography-forming tills in the lower Pechora basin and the limit of the last ice sheet. *Trudy Institute of Geology, Komi Branch of the Academy of Sciences USSR 54*, 97–107 (in Russian).

Haesaerts, P., Chekha, V. P., Damblon, F., Drozdov, N. I., Orlova, L. A. & van der Plicht, J. 2005: The loess-palaeosol succession of Kurtak (Yenisei basin, Siberia): A reference record for the Karga stage (MIS 3). *Quaternaire 16*, 3–24.

Hancock, G. J. & Murray, A. S. 1996: Source and distribution of dissolved radium in the Bega River estuary, Southeastern Australia. *Earth and Planetary Science Letters 138*, 145–155.

Heiri, O., Lotter, A. F. & Lemcke, G. 2001: Loss on ignition as a method for estimating organic and carbonate content in sediments: Reproducibility and comparability of results. *Journal of Paleolimnology 25*, 101–110.

Helmens, K. F., Räsänen, M. E., Johansson, P. W., Jungner, H. & Korjonen, K. 2000: The last interglacial–glacial cycle in NE Fennoscandia: A nearly continuous record from Sokli (Finnish Lapland). *Quaternary Science Reviews 19*, 1605–1623.

Henriksen, M., Mangerud, J., Maslenikova, O., Matiouchkov, A. & Tveranger, J. 2001: Weichselian stratigraphy and glaciotectonic deformation along the lower Pechora River, Arctic Russia. *Global and Planetary Change 31*, 297–319.

Henriksen, M., Mangerud, J., Matiouchkov, A., Paus, A. & Svendsen, J. I. 2003: Lake stratigraphy implies an 80 000 yr delayed melting of buried dead ice in northern Russia. *Journal of Quaternary Science 18*, 663–679.

Houmark-Nielsen, M., Demidov, I., Funder, S., Grøsfjeld, K., Kjær, K. H., Larsen, E., Lavrova, N., Lyså, A. & Nielsen, J. K. 2001: Early and Middle Valdaian glaciations, ice-dammed lakes and periglacial interstadials in northwest Russia: New evidence for the Pyoza River area. *Global and Planetary Change 31*, 215–237.

Hubberten, H. W., Andreev, A., Astakhov, V. I., Demidov, I., Dowdeswell, J. A., Henriksen, M., Hjort, C., Houmark-Nielsen, M., Jakobsson, M., Kuzmina, S., Larsen, E., Lunkka, J. P., Lyså, A., Mangerud, J., Möller, P., Saarnisto, M., Schirrmeister, L., Sher, A. V., Siegert, C., Siegert, M. J. & Svendsen, J. I. 2004: The periglacial climate and environment in northern Eurasia during the last glaciation (LGM). *Quaternary Science Reviews 23*, 1333–1357.

Jensen, M., Larsen, E., Demidov, I. N., Funder, S. & Kjær, K. H. 2006: Depositional environments and sea-level changes deduced from Middle Weichselian tidally influenced sediments, Arkhangelsk region, NW Russia. *Boreas 35*, 521–538.

Kaland, P. E. & Natvik, Ø. 1993: CORE 2.0, a computer program for stratigraphical data, developed at University of Bergen, Norway. Unpublished.

Kjær, K. H., Demidov, I., Larsen, E., Murray, A. & Nielsen, J. K. 2003: Mezen Bay – a key area for understanding Weichselian glaciations in northern Russia. *Journal of Quaternary Science 18*, 73–93.

Krinner, G., Mangerud, J., Jakobsson, M., Crucifix, M., Ritz, C. & Svendsen, J. I. 2004: Enhanced ice sheet growth in Eurasia owing to adjacent ice-dammed lakes. *Nature 427*, 429–432.

Kukla, G. J., Bender, M. L., de Beaulieu, J. L., Bond, G., Broecker, W. S., Cleveringa, P., Gavin, J. E., Herbert, T. D., Imbrie, J., Jouzel, J., Keigwin, L. D., Knudsen, K. L., McManus, J. F., Merkt, J., Muhs, D. R. & Müller, H. 2002: Last interglacial climates. *Quaternary Research 58*, 2–13.

Larsen, E., Kjær, K. H., Demidov, I. N., Funder, S., Grøsfjeld, K., Houmark-Nielsen, M., Jensen, M., Linge, H. & Lyså, A. 2006: Late Pleistocene glacial and lake history of northwestern Russia. *Boreas 35*, 394–424.

Larsen, E., Lyså, A., Demidov, I., Funder, S., Houmark-Nielsen, M., Kjær, K. H. & Murray, A. S. 1999: Age and extent of the Scandinavian ice sheet in northwest Russia. *Boreas 28*, 115–132.

Lemmen, D. S., Gilbert, R., Smol, J. P. & Hall, R. I. 1988: Holocene sedimentation in glacial Tasikutaaq Lake, Baffin Island. *Canadian Journal of Earth Sciences 25*, 810–823.

Mangerud, J., Astakhov, V. I., Murray, A. & Svendsen, J. I. 2001: The chronology of a large ice-dammed lake and the Barents–Kara ice sheet advances, northern Russia. *Global and Planetary Change 31*, 321–336.

Mangerud, J., Astakhov, V. & Svendsen, J. I. 2002: The extent of the Barents–Kara ice sheet during the Last Glacial Maximum. *Quaternary Science Reviews 21*, 111–119.

Mangerud, J., Jakobsson, M., Alexanderson, H., Astakhov, V., Clarke, G. K. C., Henriksen, M., Hjort, C., Krinner, G., Lunkka, J. P., Möller, P., Murray, A., Nikolskaya, O., Saarnisto, M. & Svendsen, J. I. 2004: Ice-dammed lakes and rerouting of the drainage of Northern Eurasia during the last glaciation. *Quaternary Science Reviews 23*, 1313–1332.

Mangerud, J., Svendsen, J. I. & Astakhov, V. 1999: Age and extent of the Barents and Kara ice sheet in northern Russia. *Boreas 28*, 46–80.

Miller, G. H., Mode, W. N., Wolfe, A. P., Sauer, P. E., Bennike, O., Forman, S. L., Short, S. K. & Stafford Jr., T. W. 1999: Stratified interglacial lacustrine sediments from Baffin Island, Arctic Canada:

chronology and paleoenvironmental implications. *Quaternary Science Reviews 18*, 789–810.

Moore, W. S. 1992: Radionuclides of the uranium and thorium decay series in estuarine environments. *In* Ivanovich, M. & Harmon, R. S. (eds.): *Uranium Series Disequilibrium: Applications to Environmental Problems*, 145–164. Clarendon Press, Oxford.

Murray, A. S. & Funder, S. 2003: Optically stimulated luminescence dating of a Danish Eemian coastal marine deposits: A test of accuracy. *Quaternary Science Reviews 22*, 1177–1183.

Murray, A. S. & Olley, J. M. 2002: Precision and accuracy in the optically stimulated luminescence dating of sedimentary quartz. *Geochronometria 21*, 1–16.

Murray, A. S. & Wintle, A. G. 2000: Luminescence dating of quartz using an improved single-aliquot regenerative-dose protocol. *Radiation Measurements 32*, 57–73.

Murray, A. S., Marten, R., Johnston, A. & Martin, P. 1987: Analysis for naturally occurring radionuclides at environmental concentrations by gamma spectrometry. *Journal of Radioanalytical and Nuclear Chemistry, Articles 115*, 263–288.

Murray, A. S., Svendsen, J. I., Mangerud, J. & Astakhov, V. I. 2007: Testing the accuracy of quartz OSL dating using a known-age Eemian site on the river Sula, northern Russia. *Quaternary Geochronology 2*, 102–109.

Nalivkin, D. V. 1973: *Geology of the U.S.S.R.* 855 pp. Oliver & Boyd, Edinburgh.

National Snow and Ice Data Center 2006: *Monthly Mean Precipitation Sums at Russian Arctic Stations, 1966–1990*. Boulder, Colorado, USA. Available at: http://www.nsidc.org/data/docs/noaa/g02170_russian_monthly_precip/index.html.

Olley, J. M. & Murray, A. S. 1994: The origins of variability of in the $^{230}Th/^{232}Th$ ratio in sediments. *IAHS Publication 224*, 65–70.

Olley, J. M., Murray, A. S. & Roberts, R. G. 1996: The effects of disequilibria in the uranium and thorium decay chains on burial dose rates in fluvial sediments. *Quaternary Science Reviews 15*, 751–760.

Pachukovsky, V. M., Plyakin, A. M., Graf, V. I., Oparenkov, N. V., Kokin, P. N., Kopytin, A. S., Nikitin, N. S., Lyutoyev, A. A. & Lebedeva, G. K. 1978: Geological mapping report of scale 1:50000 of Middle Timan (Quadrangles Q-39-101-A, B, V, G, 102-V, 112-B, G, 113-A, B, V, G, 114-A, V, G, 115-V, 125-B, G, 126-A, B, V, G, 127-A, V, 138-A, B, 139-A). Russian Geological Survey, Ukhta (in Russian).

Paus, A. 1995: The Late Weichselian and early Holocene tree-birch history in S Norway and the Bølling *Betula* time-lag in NW Europe. *Review of Palaeobotany and Palynology 85*, 243–262.

Paus, A., Svendsen, J. I. & Matiouchkov, A. 2003: Late Weichselian (Valdaian) and Holocene vegetation and environmental history of the northern Timan Ridge, European Arctic Russia. *Quaternary Science Reviews 22*, 2285–2302.

Pavlov, P., Svendsen, J. I. & Indrelid, S. 2001: Human presence in the European Arctic nearly 40,000 years ago. *Nature 413*, 64–67.

Polyak, L., Gataullin, V., Okuneva, O. & Stelle, V. 2000: New constrains on the limits of the Barents–Kara ice sheet during the Last Glacial Maximum based on borehole stratigraphy from the Pechora Sea. *Geology 28*, 611–614.

Reimer, P. J., Baillie, M. G. L., Bard, E., Bayliss, A., Beck, J. W., Bertrand, C., Blackwell, P. G., Buck, C. E., Burr, G., Cutler, K. B., Damon, P. E., Edwards, R. L., Fairbanks, R. G., Friedrich, M., Guilderson, T. P., Hughen, K. A., Kromer, B., McCormac, F. G., Manning, S., Ramsey, C. B., Reimer, R. W., Remmele, S., Southon, J. R., Stuiver, M., Talamo, S., Taylor, F. W., van der Plicht, J. & Weyhenmeyer, C. E. 2004: IntCal04 Terrestrial Radiocarbon Age Calibration, 0–26 Cal Kyr BP. *Radiocarbon 46*, 1029–1058.

Seidenkrantz, M. S., Bornmalm, L., Johnsen, S. J., Knudsen, K. L., Kuijpers, A., Lauritzen, S. E., Leroy, S. A. G., Mergeai, I., Schweger, C. & van Vliet-Lanoë, B. 1996: Two-step deglaciation at the oxygen isotope stage 6/5e transition: the Zeifen–Kattegat climate oscillation. *Quaternary Science Reviews 15*, 63–75.

Semenenko, L. T., Alyoshinskaya, Z. V., Arslanov, K. A., Valuyeva, M. N. & Krasnovskaya, F. I. 1981: Upper Pleistocene section near 'First of May' Factory in Dmitrov district, Moscow region (sediments of the former Tatischevo Lake). *In: Novye dannye po stratigrafii i paleogeografii verkhnego pliotsena i pleistosena tsentralnykh rayonov evropeiskoi chasti, SSSR (for XI Congress INQUA, Moscow, 1982)*, 121–135. Nauka, Moscow.

Siegert, M. J. & Marsiat, I. 2001: Numerical reconstructions of LGM climate across the Eurasian Arctic. *Quaternary Science Reviews 20*, 1595–1605.

Stockmarr, J. 1971: Tablets with spores in absolute pollen analysis. *Pollen et Spores 13*, 615–621.

Svendsen, J. I., Alexanderson, H., Astakhov, V. I., Demidov, I., Dowdeswell, J. A., Funder, S., Gataullin, V., Henriksen, M., Hjort, C., Houmark-Nielsen, M., Hubberten, H. W., Ingólfsson, Ó., Jakobsson, M., Kjær, K. H., Larsen, E., Lokrantz, H., Lunkka, J. P., Lyså, A., Mangerud, J., Matiouchkov, A., Murray, A., Möller, P., Niessen, F., Nikolskaya, O., Polyak, L., Saarnisto, M., Siegert, C., Siegert, M. J., Spielhagen, R. F. & Stein, R. 2004: Late Quaternary ice sheet history of northern Eurasia. *Quaternary Science Reviews 23*, 1229–1271.

Tveranger, J., Astakhov, V. & Mangerud, J. 1995: The margin of the last Barents–Kara Ice Sheet at Markhida, northern Russia. *Quaternary Research 44*, 328–340.

Tveranger, J., Astakhov, V., Mangerud, J. & Svendsen, J. I. 1998: Signature of the last shelf-centered glaciation at a key section in the Pechora Basin, Arctic Russia. *Journal of Quaternary Science 13*, 189–203.

Velichko, A. A., Andreev, A. A. & Klimanov, V. A. 1997: Climate and vegetation dynamics in the tundra and forest zone during the late glacial and Holocene. *Quaternary International 41/42*, 71–96.

Velichko, A. A., Bogucki, A. B., Morozova, T. D., Udartsev, V. P., Khalcheva, T. A. & Tsatskin, A. I. 1984: Periglacial landscapes of the East European Plain. *In* Velichko, A. A. (ed.): *Late Quaternary Environments of the Soviet Union*, 95–118. University of Minnesota Press, Minneapolis.

Velichko, A. A., Faustova, M. A., Gribchenko, Yu. N., Pisareva, V. V. & Sudakova, N. G. 2004: Glaciations of the East European Plain – distribution and chronology. *In* Ehlers, J. & Gibbard, P. L. (eds.): *Quaternary Glaciations – Extent and Chronology. Vol. 1. Europe*, 337–354. Elsevier, Amsterdam.

Watanuki, T., Murray, A. S. & Tsukamoto, S. 2005: Quartz and polymineral luminescence dating of Japanese loess over the last 0.6 Ma: Comparison with an independent chronology. *Earth and Planetary Science Letters 240*, 774–789.

Zelikson, E. M. 1995: Vegetation of eastern Europe during interstadial and interglacials of the Middle and Late Pleistocene. *In* Velichko, A. A. (ed.): *Climate and Environment Changes of East Europe during the Holocene and Late–Middle Pleistocene*, 80–92. Institute of Geography of Russian Academy of Sciences, Moscow.